
Article:
Morsli, S. orcid.org/0000-0002-0371-0732, Henriques, C.M. orcid.org/0000-0003-1882-756X, Ellis, P.S. et al. (5 more authors) (2023) A p21-GFP zebrafish model of senescence for rapid testing of senolytics in vivo. Aging Cell. e13835. ISSN 1474-9718

https://doi.org/10.1111/acel.13835

Received: 20 December 2022 | Revised: 19 March 2023 | Accepted: 21 March 2023

DOI: 10.1111/acel.13835

Aging Cell WILEY

RESEARCH ARTICLE

A p21-GFP zebrafish model of senescence for rapid testing of senolytics in vivo

Samir Morsli[1,2,3,4] | Catarina M. Henriques[1,2,3] | Pamela S. Ellis[1,3] | Heather Mortiboys[2,4] | Sarah Baxendale[1,2,5] | Catherine A. Loynes[1,6] | Stephen A. Renshaw[1,2,6] | Ilaria Bellantuono[2,3]

[1]The Bateson Centre, University of Sheffield, Western Bank, Sheffield, S10 2TH, UK

[2]Healthy Lifespan Institute, University of Sheffield, Western Bank, Sheffield, S10 2TH, UK

[3]Department of Oncology and Metabolism, University of Sheffield, Beech Hill Road, Sheffield, S10 2RX, UK

[4]Sheffield Institute for Translational Neuroscience, Department of Neuroscience, University of Sheffield, 385a Glossop Road, Sheffield, S10 2HQ, UK

[5]School of Biosciences, University of Sheffield, Sheffield, S10 2TH, UK

[6]Department of Infection, Immunity and Cardiovascular Disease, University of Sheffield, Beech Hill Road, Sheffield, S10 2RX, UK

Correspondence
Ilaria Bellantuono, Department of Oncology and Metabolism, The Healthy Lifespan Institute, D Floor, The Medical School, Beech Hill Road, Sheffield S10 2RX, UK.
Email: i.bellantuono@shef.ac.uk

Stephen A. Renshaw, Department of Infection, Immunity and Cardiovascular Disease, The Medical School, Beech Hill Road, Sheffield S10 2RX, UK.
Email: s.a.renshaw@sheffield.ac.uk

Present address
Samir Morsli, Early Cancer Institute, University of Cambridge, Hutchison Building, Cambridge, CB2 0XZ, UK

Funding information
Biotechnology and Biological Sciences Research Council, Grant/Award Number: BB/M011151/1

Abstract

Senescence drives the onset and severity of multiple ageing-associated diseases and frailty. As a result, there has been an increased interest in mechanistic studies and in the search for compounds targeting senescent cells, known as senolytics. Mammalian models are commonly used to test senolytics and generate functional and toxicity data at the level of organs and systems, yet this is expensive and time consuming. Zebrafish share high homology in genes associated with human ageing and disease. They can be genetically modified relatively easily. In larvae, most organs develop within 5 days of fertilisation and are transparent, which allows tracking of fluorescent cells in vivo in real time, testing drug off-target toxicity and assessment of cellular and phenotypic changes. Here, we have generated a transgenic zebrafish line that expresses green fluorescent protein (GFP) under the promoter of a key senescence marker, p21. We show an increase in p21:GFP$^+$ cells in larvae following exposure to ionising radiation and with natural ageing. p21:GFP$^+$ cells display other markers of senescence, including senescence-associated β-galactosidase and IL6. The observed increase in senescent cells following irradiation is associated with a reduction in the thickness of muscle fibres and mobility, two important ageing phenotypes. We also show that quercetin and dasatinib, two senolytics currently in clinical trials, reduce

Abbreviations: 7AAD, 7-Aminoactinomycin D; BAC, bacterial artificial chromosome; D, dasatinib; dpf, day post-fertilization; FACS, fluorescence activated cell sorting; FBS, foetal bovine serum; GFP, green fluorescent protein; ISH, in situ hybridization; Mo, months; p21:GFP, TgBAC(cdkn1a:GFP)sh506; PCNA, proliferating cell nuclear antigen; Q, quercetin; SASP, senescence induced secretory phenotype; SC, senescent cells.

All experiment were performed with permission and according to the home office licence N70/8681.

the number of p21:GFP$^+$ cells, in a rapid 5-day assay. This model provides an important tool to study senescence in a living organism, allowing the rapid selection of senolytics before moving to more expensive and time-consuming mammalian systems.

KEYWORDS
ageing, GFP, p21, senescence, senolytics, toxicity, transgenic, zebrafish

1 | INTRODUCTION

Senescent cells (SC) are characterised by cell-cycle arrest, loss of function (despite persisting metabolic activity) and by the secretion of multiple pro-inflammatory and tissue-remodelling factors, known as the senescence induced secretory phenotype (SASP). Senescence can be triggered by internal stimuli, including persistent DNA damage, telomere dysfunction or oncogene activation or external stimuli, such as ionising radiation (Di Micco et al., 2021). In animal models, the burden of SC increases with age in multiple tissues (Biran et al., 2017; Yousefzadeh et al., 2020), whilst their elimination improves tissue homeostasis with age, preventing the onset or limiting the severity of multiple age-associated diseases (Robbins et al., 2021). SC clearance, therefore, offers great promise for the prevention of multimorbidity and frailty, two of the biggest challenges for modern healthcare and as such, has galvanised interest in developing new drugs to reduce the burden of SC.

However, there are major challenges impeding mechanistic studies and testing of compounds to reduce senescent cell burden. In vitro systems do not provide the same level of information on toxicity, cell–cell and organ–organ interaction as animal models, yet the use of in vivo mammalian systems takes significant time and resources. Zebrafish models can often bridge the gap between in vitro systems and in vivo mammalian systems. Zebrafish share 84% of known human disease-associated genes and 70% of human protein encoding genes (Howe et al., 2013) and have unique features as a model organism. They are born in large clutches and grow quickly, rapidly providing high numbers at low cost. Larval zebrafish are almost completely optically transparent and amenable to genetic manipulation, allowing ready generation of fluorescent transgenic reporters to track individual cells within the same live animal, over time. By combining different fluorescent reporters, it becomes possible to image the interaction between cell types and elucidate novel mechanisms, as has been shown with labelling of cells of the innate immune system (Ellett et al., 2011; Renshaw et al., 2006). Numerous zebrafish models of disease are available, and several have been shown to be amenable to studying drug efficacy in vivo (Bradford et al., 2017). Zebrafish larvae fit in 96-well plates and can be assessed for potential off-target toxicity and cellular and phenotypic changes across multiple tissues, using assays which last only a few days. For example, with automated quantitation, more than 500,000 zebrafish larvae were screened to identify novel compounds that increase the number of insulin-producing β-cells in the pancreas, as a potential treatment for diabetes. (Wang et al., 2015)

In this study, we report the generation of a transgenic zebrafish line *TgBAC(cdkn1a:GFP)sh506* (termed p21:GFP thereafter), which expresses Green Fluorescent Protein (GFP) under the promoter of a key senescence marker, p21 (*cdkn1a*). p21 is one of the major regulators and cellular markers of senescence (Estela González-Gualda et al., 2021). Zebrafish have a homologue of the human p21 gene, known to increase with increased levels of p16-like expression and senescence-associated β-galactosidase (Da Silva-Álvarez et al., 2020). In contrast, the zebrafish orthologue for p16 is also an orthologue for p15 and p19 (Shim et al., 2017). For this reason, we have focussed on generating a transgenic line for p21. Recent reports show that cells expressing high levels of p21 in vivo express other markers of senescence and their numbers increase with age, in multiple murine organs (Wang et al., 2021). In addition, elimination of p21$^+$ SC reduces frailty and attenuates insulin resistance in obese mice (Wang et al., 2022), whilst elimination of p21$^+$ cells, but not p16$^+$ cells, improves radiation-induced osteoporosis (Chandra et al., 2022), suggesting that p21 is a good marker of SC.

Here, we demonstrate that expression of p21-GFP is upregulated in larvae following exposure to ionising radiation and with natural ageing. Importantly, accumulation of SC is associated with reduction in muscle fibre thickness and mobility, two important ageing phenotypes. We have identified a population of cells that express high levels of p21:GFP (p21:GFP^{bright}) and co-express other markers of senescence, including IL6, a major SASP factor. Finally, we show that the p21:GFP transgenic zebrafish line can be used for imaging and serves as a useful readout of senescence when testing for the most effective senolytic drugs in vivo, using 96-well plates in a rapid 5-day assay. This line, therefore, provides an important tool to study SC in a living organism, allowing for the rapid testing of drugs, before moving to more expensive and time-consuming mammalian systems. Importantly, the use of zebrafish less than 5 day post-fertilization (dpf) fulfils the principle of the 3Rs as these animals are considered protected under the animals (scientific procedures) Act, and their use could replace high-order animals.

2 | RESULTS

2.1 | Zebrafish larvae show markers of senescence following ionising radiation

To determine whether it was possible to induce senescence in zebrafish larvae, we exposed the larvae to 12 Gy irradiation at 2 dpf

(Figure 1a). These parameters were chosen because they were the highest dose and the earliest time point possible that did not result in an abnormal development or reduced viability (Figure S1). Abnormal development was assessed by counting the number of abnormalities (scored as pericardial oedema, deflated swim bladder, spinal curvature, skin lesions and stunted growth) in 140 fish over 3 experiments. The percentage of abnormalities scored in the non-irradiated group was 10.2 ± 6.6%, with no significant difference across the 3 days. There were significantly more abnormalities by 5 dpf in zebrafish larvae irradiated at 1 dpf (64 ± 13.2%). However, the number of abnormalities by 5 dpf were in a similar range to non-irradiated zebrafish larvae when the irradiation was performed at day 2 (15 ± 4.6%) or at day 3 (19.6 ± 8.7). Therefore, we chose to irradiate at 2 dpf from here on. Multiple markers of senescence were assessed at 5 dpf. We observed a significant increase in the expression of mRNA for *p21* ($p = 0.0005$, $n = 4$), *p16-like* (*cdkn2a/b*; $p = 0.0002$, $n = 4$), *p53* ($p = 0.0002$, $n = 4$), *cyclinG1* ($p = 0.008$, $n = 3$) and SASP factor *mmp2* ($p = 0.0005$, $n = 4$) by qPCR, using whole fish RNA extracts from 50 pooled larvae in each experiment (Figure 1b). No significant increase in the levels of SASP marker *il-8* was observed (Figure 1b). To determine the spatial location of SC, we performed whole-mount in situ hybridisation using a previously published *p21* probe (Laranjeiro et al., 2013). We observed a significant increase in *p21* expression following irradiation, which increased in a dose-dependent manner (Figure 1c). The same dose-dependent response increase was detected by RT-qPCR (Figure 1d). The increase was particularly strong in the pharyngeal arches, brain and intestinal regions of the zebrafish and overlapped with areas where there was an increase in senescence-associated βGal expression (SA-βGal) (Figure 1e and Figure S2). Immunostaining for γH2AX DNA damage foci, another marker of senescence, showed a significant increase in the percentage of cells with bright nuclear γH2AX staining (individual foci were not distinguishable) in the ventral head region, following irradiation (Figure 1f). These ranged from 3% to 10%, comparable to the levels seen in aged organisms (Dehkordi et al., 2021; Jurk et al., 2014; Ogrodnik et al., 2017).

2.2 | Irradiated larvae show signs of muscle wasting similar to aged zebrafish

One of the characteristics of ageing across organisms, including humans, and one of the main signs of frailty, is loss of body mass associated with muscle wasting (Cesari et al., 2006). In order to assess whether irradiation caused changes in muscle phenotype, we performed histological analysis of muscle in the ventral region of zebrafish larvae at 12 dpf following 12 Gy of irradiation. There was a significant decrease in muscle fibre thickness compared to the non-irradiated control. This was similar to the decrease observed with natural ageing in the muscle of middle-aged (18 months) and geriatric fish (>36 months) (Figure 2a). More importantly, when larvae were placed individually in a 24-well plate and their movement quantified over a 30-min period, at 5 and 12 dpf, we observed a significant reduction in the distance travelled at both time points in irradiated larvae, compared to non-irradiated larvae (Figure 2b). These data suggest that irradiated larvae develop similar muscle changes to aged zebrafish and that histological changes in muscle fibre thickness were accompanied by loss of muscle function.

2.3 | Generation of a p21:GFP Zebrafish model

To generate a p21:GFP reporter transgenic line, we used the DKEY 192-O24 bacterial artificial chromosome (BAC) encompassing the *p21* locus and containing at least 100 kbp downstream and 50 kbp upstream of the start codon, to include as much of the promoter and regulatory regions of the gene as possible (Figure S3a). The BAC was modified such that the GFP sequence was incorporated into the BAC at the initial ATG start codon of the *p21*-encoding region in the first exon, common to both *p21* splice variants, and thereby placed under regulation of the *p21*-promoter (Figure S3b). The insertion of GFP disrupted the expression of the *p21* gene contained in the BAC and ensured it did not express an extra copy of *p21* when inserted into the zebrafish genome. To improve the likelihood that the modified BAC was incorporated into the zebrafish genome, a transposon-mediated system was used (Suster et al., 2011; Figure S3c,d).

To verify that GFP expression was regulated in a similar way to endogenous p21, we measured green fluorescence intensity following 12 Gy irradiation. An increase in mean fluorescent intensity was observed post-irradiation, which was more pronounced in the intestine, head regions and pharyngeal arches (Figure 3a), similar to that observed using in situ hybridisation and a p21 probe (Figure 3b). To verify that the transgenic reporter had comparable endogenous *p21* expression to wild-type fish and there was no additional contribution from the BAC *p21* mRNA expression levels was assessed by qPCR in the whole p21:GFP zebrafish at 3 days post-irradiation. As expected, we found an increase in p21 expression with irradiation in both wild-type and transgenic animals but there was no difference in levels of expression between the two lines (Figure 3c), suggesting that there was no additional p21 expression due to the presence of the BAC.

2.4 | The number of p21:GFP^{bright} Cells increases with irradiation and natural ageing

To quantify the number of p21:GFP^{+} cells, flow cytometric analysis of zebrafish larvae post-irradiation was performed at 5 and 12 dpf using the gating strategy shown in Figure S4. Before irradiation, we noticed a population of p21:GFP^{dim} cells at 5 dpf (23.3% ± 3.4%, $n = 3$; Figure 3d), which did not significantly increase following irradiation when compared to the non-irradiated zebrafish larvae and remained consistent at later time points. In contrast, we detected the appearance of a GFP^{bright} population of cells at 5 dpf following irradiation (0.95% ± 0.01% vs 14.06% ± 1.01% for 0 and 12 Gy, respectively, $n = 3$ $p < 0.05$, Figure 3d). The presence of this GFP^{bright} population

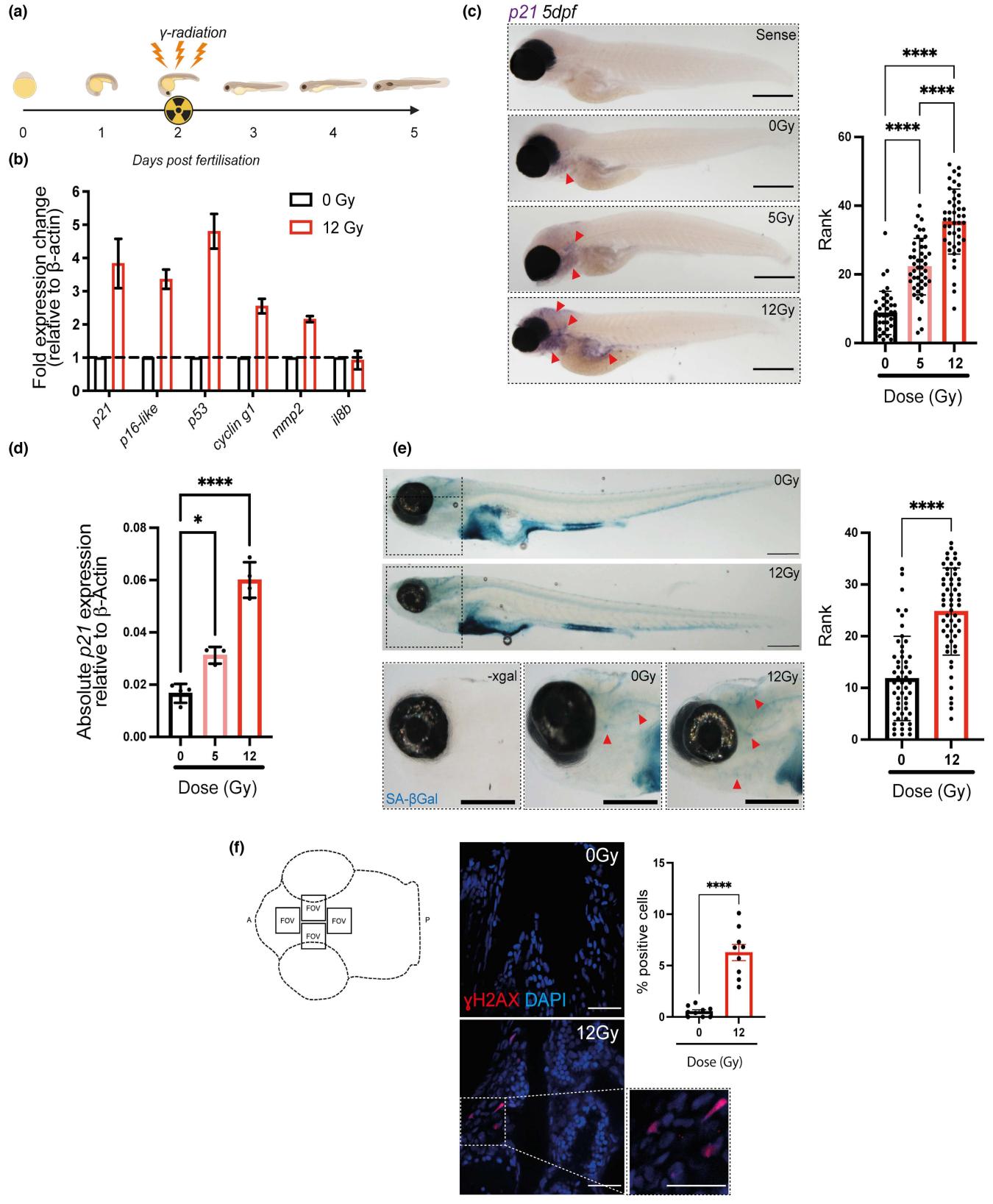

persisted in the irradiated zebrafish larvae at 12 dpf (1.03%±0.05% vs 6.65%±0.72% 0 vs 12 Gy, respectively, $n=3$, $p<0.05$) although at lower levels than that observed at 5 dpf (Figure 3e). Recently, Wang et al. (2022) also reported a population of p21GFP^{high} cells accumulating in multiple tissues with age using an inducible p21-cre GFP mouse model. Indeed, analysis of brain, intestine and liver of middle-aged and geriatric zebrafish also showed a significant increase in p21:GFP^{bright} cells whereas no statistical difference

FIGURE 1 Irradiation of zebrafish larvae upregulates multiple markers of senescence. (a) Diagram depicting the experimental protocol used to induce senescence in zebrafish larvae using Cs_{137} ɣ-Irradiation at 2 dpf and assessing markers of senescence at 5 dpf. (b) Quantitative PCR (qPCR) of whole zebrafish mRNA at 5 dpf following 12 Gy irradiation to determine gene expression of *p21 (cdkn1a)*, *p16-like (cdkn2a/b)*, *p53*, *cyclin-g1*, *mmp2 and IL8b*. Fold expression was calculated by $2^{-\Delta Ct}$ relative to β-actin. mRNA was pooled from 50 zebrafish for each independent repeat. The graph represents the mean ± SEM of 3 repeats. (c) Transmitted light photomicrographs of a whole-mount in situ hybridisation (WISH) for *p21* (*cdkn1a*) mRNA expression at 5 dpf following 5 or 12 Gy irradiation at 2 dpf (left panels). Areas of increased staining include pharyngeal arches, brain and intestine, depicted with red arrows. Scale 250 μm. Quantification of ISH photomicrographs through blind ranking such that fish with the strongest staining are ranked highest (right panel). Data were examined by Kruskal–Wallis test with Dunn's multiple comparisons ($N = 45$). (d) Quantitative qPCR of whole zebrafish mRNA at 5 dpf following irradiation at 5 and 12 Gy to determine expression of p21. Data expressed as expression relative to GAPDH and analysed by one-way ANOVA and Sidak's multiple comparisons test. (e) Photomicrographs of zebrafish at 5 dpf stained for senescence-associated β-Galactosidase (SA-βGal) activity. Representative examples of the head region are also displayed on the left. Scale 200 μm (Left panels). Quantification of SA-βGal activity in the head region by blind ranking is on the left ($n = 55$) (right panel). Data were examined by Kruskal–Wallis test with Dunn's multiple comparisons (f) Confocal fluorescence photomicrographs (Scale 25 μm) and quantification of γH2AX immunofluorescence in the ventral zebrafish head regions (areas depicted in the cartoon in the left panel) a minimum of 600 cells/fish were counted. For each fish, 4 fields of view and 3 individual z planes, 10 μM apart were analysed. At least 9 fish were analysed across three independent repeats. Data represented as mean ± SEM ($N = 9$) and examined by unpaired *t*-test. Significant differences displayed as $^{**}p < 0.01$; $^{****}p < 0.0001$. a, Anterior; p, posterior; FOV, field of view.

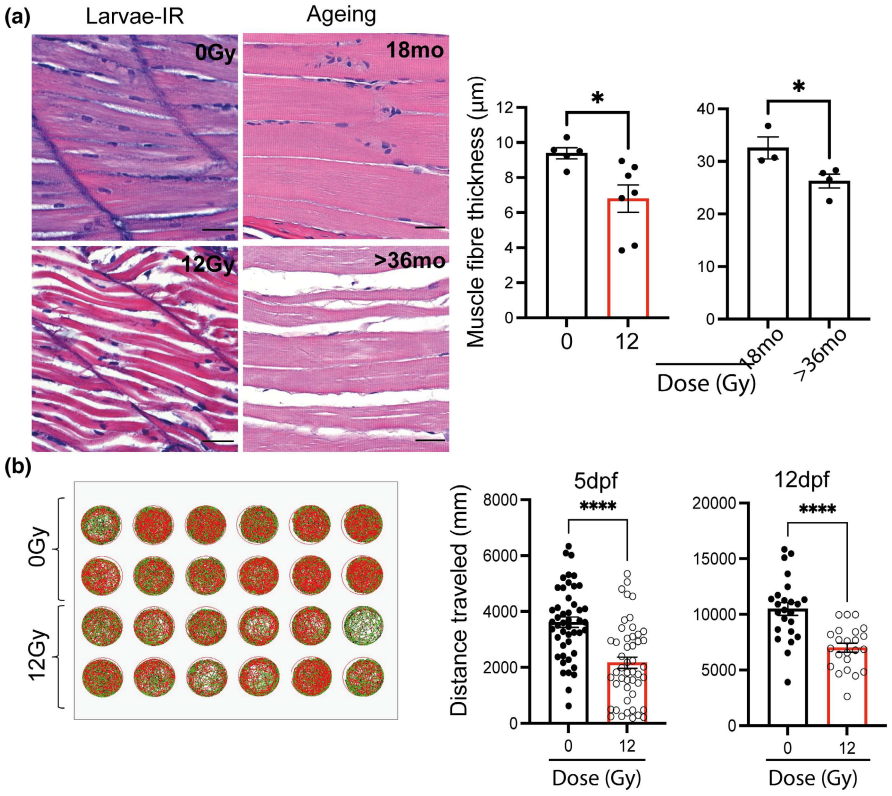

FIGURE 2 Zebrafish larvae showed reduced muscle fibre thickness and mobility following irradiation. (a) Representative photomicrographs of haematoxylin and eosin (H&E) staining of zebrafish muscle from either 12 dpf larvae with and without irradiation (top left panel), and middle aged and geriatric adults (bottom left panel) (scale 25 μm) and quantification of muscle fibre thickness in larvae following irradiation and in middle aged (18 months) and geriatric zebrafish (>36 months) (right panels). Data shown as mean ± SEM. Each dot represents an animal. (b) Representative example of distance travelled by zebrafish over 30 min in a 24-well plate at 5 ($N \geq 47$) and 12 dpf ($N \geq 23$) following 0 Gy or 12 Gy irradiation administered at 2 dpf and quantitation of the distance travelled at 5 and 12 dpf. Each dot represents an animal. Data examined by unpaired *t*-test. $^{****}p < 0.0001$; $^{*}p < 0.05$.

was observed in the p21:GFP^{dim} cells (Figure 3f). Notably, tissues showed time and tissue-specific increases in the accumulation of SC with age. Whilst the intestine showed a significant increase at middle age, the brain showed a more progressive increase through the ages and the liver seems to suffer a significant increase mainly at geriatric age (Figure 3f). This is in line with the findings of Carneiro et al. (2016), Henriques et al. (2013) where a time and tissue-specific degeneration was observed with ageing wild-type zebrafish and was accelerated in the prematurely aged telomerase mutant (*tert*$^{-/-}$) zebrafish. The intestine was one of the first tissues to degenerate and accumulate senescence.

2.5 | P21:GFP^{bright} cells show multiple markers of senescence

To verify that p21:GFP^{+} cells co-expressed other known markers of senescence, p21:GFP zebrafish larvae were exposed to 12 Gy irradiation at 2 dpf and p21:GFP^{+} cells were subjected to fluorescence activated cell sorting (FACS) at 5 and 12 dpf. Cells showed over 90% purity following FACS sorting (Figure 4a). Following irradiation, p21:GFP^{bright} but not p21:GFP^{dim} cells showed a significant increase in size and granularity, which are features of senescence, compared to those not exposed to irradiation (Figure 4b–d). In addition, a

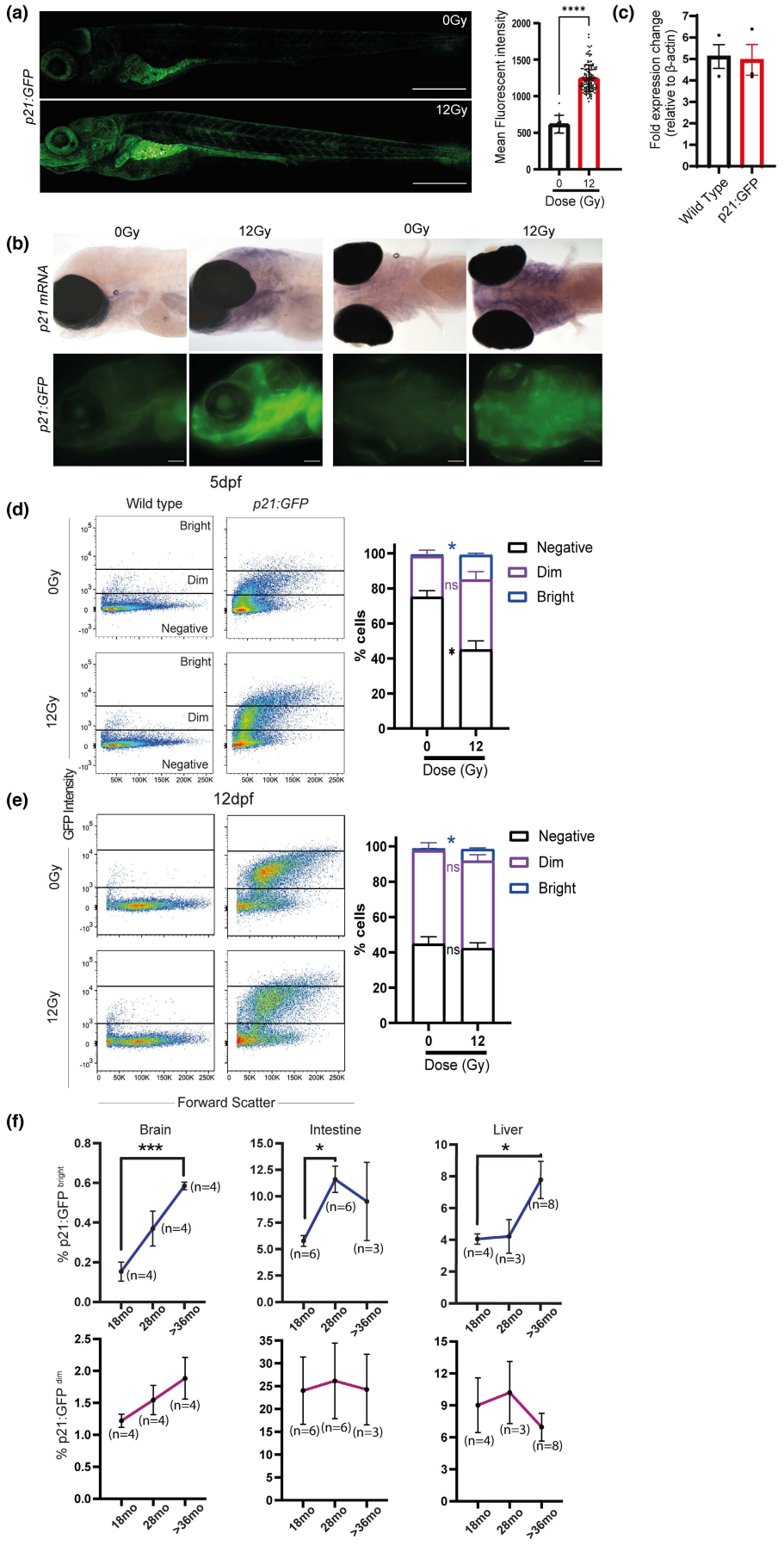

FIGURE 3 *p21:GFP*^{Bright} cells are induced with irradiation and ageing in the p21:GFP transgenic zebrafish. (a) Representative confocal fluorescence photomicrographs to depict GFP fluorescence of 5 dpf *p21:GFP* zebrafish following 0 Gy or 12 Gy irradiation at 2 dpf (Scale 500 μm) and quantification of fluorescence intensity of the whole p21:GFP transgenic zebrafish. Each dot represents an animal. Graph represents Mean ± SEM and data were examined by Mann–Whitney test. (b) Transmitted and wide-field fluorescence photomicrographs taken laterally and ventrally showing p21:GFP fluorescence recapitulated endogenous *p21* mRNA expression (Scale bar 100 μm). (c) qPCR of whole zebrafish mRNA demonstrating *p21* expression in transgenic *p21:GFP* and wild-type strain zebrafish, relative to βactin ($2^{-\Delta Ct}$). mRNA was pooled from 50 zebrafish for each independent repeat. The graph represents the mean ± SEM of 3 repeats. Data were examined by 2 way ANOVA with Tukey's multiple comparison test. ****$p < 0.0001$; ***$p < 0.001$; **$p < 0.01$ (d) Representative flow cytometry profiles of dissociated 5 dpf p21:GFP zebrafish and wild-type siblings treated with either 0 Gy or 12 Gy irradiation and quantitation of the proportion of live p21:GFP-, p21:GFP^{Dim} and p21:GFP^{Bright} cells in dissociated 5 dpf *p21*:GFP zebrafish larvae. Dissociated cells from 50 fish were pooled for each repeat ($n = 3$) (e) Representative flow cytometry profiles of dissociated 12 dpf *p21*:GFP zebrafish larvae and wild-type siblings treated with either 0 Gy or 12 Gy irradiation. Quantification of the proportion of live p21:GFP-, p21:GFP^{Dim} and p21:GFP^{Bright} cells in dissociated 12 dpf *p21*:GFP zebrafish larvae. Dissociated cells from 25 fish were pooled for each experiment ($n = 3$). Data were examined by 2 way ANOVA with Šidak's multiple comparisons test. (f) The proportion of p21:GFP^{Dim}, and p21:GFP^{Bright} at 18, 28 and at least 36 months (mo) old in adult *p21:GFP* zebrafish brains, intestines and livers were quantified. Data were examined by one-way ANOVA with Sidak's multiple comparison test. Data are presented as mean ± SEM. ***$p < 0.001$, **$p < 0.01$; *$p < 0.05$.

significant increase in cells with >5 γH2AX$^+$ foci and PCNA negative was observed in both GFP^{Bright} and GFP^{Dim} populations at 5 dpf and persisted at 12 dpf (Figure 4e–g). However, the increase was more modest in the GFP^{dim} (31.2 ± 10.1% at 5 dpf) in comparison with the GFP^{bright} population (52.2 ± 8.1% at 5 dpf; Figure 4g). No significant increase in the number of cells IL6$^+$PCNA$^-$ was observed in the GFP^{dim} population when compared to cells from non-irradiated p21:GFP fish at 5 dpf and 12 dpf (Figure 4g). This was in contrast to the GFP^{bright} population where 22.0 ± 3.5% of GFP^{bright} cells were IL6$^+$PCNA$^-$ at 5 dpf and this increased to 48.1 ± 6.7% at 12 dpf (Figure 4g). These data suggest that the p21GFP^{bright} population enriches for a population with properties of SC.

2.6 | Senolytics clear p21^{bright} cells in zebrafish

To develop an accurate way to detect p21:GFP^{bright} cells by imaging for drug testing, zebrafish were irradiated at 12 Gy at 2 dpf and transferred in a 96-well plate in medium. At 5 dpf, zebrafish were anaesthetised and imaged in a horizontal position on an Opera Phenix® High-Content Screening System. Tiled confocal photomicrographs were acquired and individual cells segregated for analysis (Figure 5a). The mean fluorescence intensity of individual cells was classified against thresholds to determine whether they were p21:GFP$^-$, p21-GFP^{Dim} or p21:GFP^{Bright}. The thresholds were established based on the level of fluorescence in the untreated wild-type zebrafish (p21:GFP$^-$) and non-irradiated p21:GFP zebrafish (p21:GFP^{dim}). To verify that these thresholds detected the correct proportion of p21:GFP^{bright} in a reproducible manner, we firstly analysed p21:GFP fish at 5 dpf in three experiments performed on three different days. We compared the reproducibility in detecting the zebrafish area considered for analysis, the number of fluorescent cells detected in each zebrafish and the the ratio of p21:GFP^{bright} cells detected per zebrafish over the total number of fluorescent cells. No significant difference was observed when the same plate was analysed on different days by the same operator (Figure S5). In addition, the number of p21GFP^{bright} cells in irradiated and non-irradiated fish was compared. As expected, we observed a significant increase in the p21:GFP^{bright} cells following irradiation (Figure 5b). Finally, the number of p21:GFP^{bright} detected by imaging was compared to those detected by flow cytometry. No significant difference was found when comparing the percentage increase in GFP^{bright} cells detected by this method and by FACS (Figure 5b), suggesting that this method is accurately measuring the increase in the number of p21:GFP^{bright} cells. To verify that known senolytics had similar effects in zebrafish to those reported in in vitro and in vivo models, p21:GFP fish were irradiated at 2 dpf and transferred to a 96-well plate in medium containing either the senolytic cocktail dasatinib (D, 500 nM) and quercetin (Q, 50 μM) or ABT-263 (navitoclax, 5 μM). DMSO was used as a vehicle control. These doses were established as the highest doses that did not cause significant acute toxicity to the fish based on key signs including pericardial oedema and abnormal spinal curvature (von Hellfeld et al., 2020). Media containing the drugs was refreshed at 4 dpf, and fish were analysed at 5 dpf. A decrease in the percentage of GFP^{bright}/total number of fluorescent cells was observed when DQ and ABT263 were administered, although this reached statistical significance only for DQ (Figure 5c).

3 | DISCUSSION

In this study, we have generated a p21:GFP zebrafish model and developed a protocol for the induction of senescence over 5 days. p21 is an important marker of senescence as shown by studies in p21:GFP mice (Wang et al., 2021). As was recently found in these mice, we have identified a population of p21:GFP^{bright} cells, which accumulate in both zebrafish larvae following irradiation and in the tissues with age and are enriched for markers of senescence. Approximately 50% of the GFP^{bright} PCNA cells show more than 5 γH2AX foci/cell and express IL6 at 5 dpf and at 12 dpf, suggesting that they are persistent. This is comparable to what has been found in the p21:GFP mice where approximately 50% of cells were found to be positive for SA-β-Gal staining (Wang et al., 2021). The percentage of p21:GFP^{bright} cells in the tissues of adult and geriatric

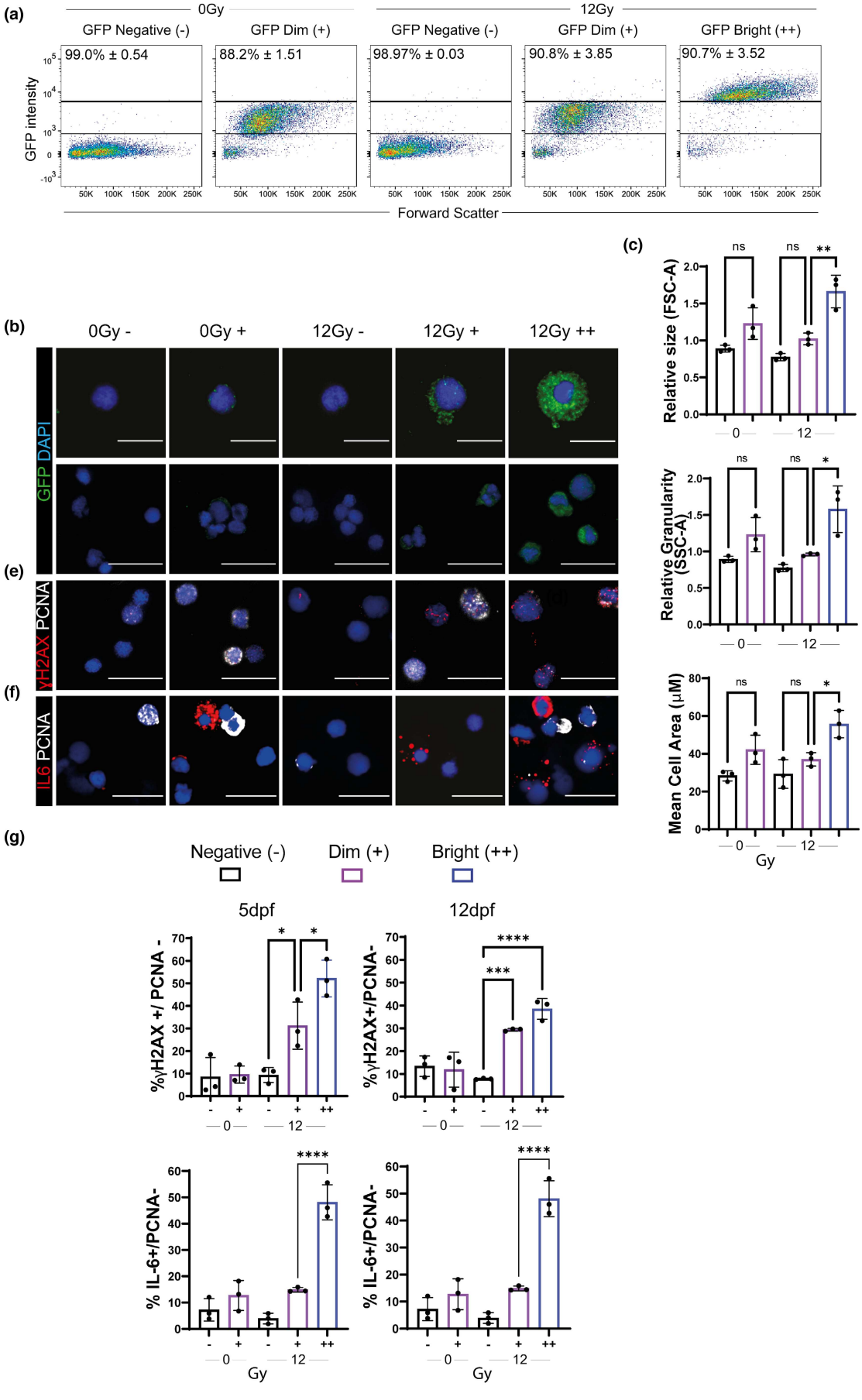

FIGURE 4 GFP^{Bright} cells are associated with other markers of senescence at 5 and 12 dpf. (a) Representative flow cytometry profiles of 5 dpf *p21:GFP* cells after sort according to GFP intensity. The level of purity of each population across three independent biological replicates is at the top of the graph. (b) Representative confocal fluorescent photomicrographs of immunofluorescence for GFP Scale 10 μm (top), 20 μm (bottom). (c) Quantification of cell size (FSC-A) and granularity (SSC-A) in GFP^{Negative}, GFP^{Dim} and GFP^{Bright} populations, relative to total live cells. (d) Mean cell area quantified by measuring confocal fluorescent photomicrographs of sorted GFP^{Negative}, GFP^{Dim} and GFP^{Bright} populations. (e,f) Representative confocal fluorescent photomicrographs of immunofluorescence for (e) γH2AX and PCNA or (f) IL6 and PCNA in 5 dpf p21:GFP cells, sorted according to GFP intensity. (f) Quantification of the proportion of γH2AX +/PCNA− cells (top) and IL6 +/PCNA− cells (bottom) in GFP^{Negative}, GFP^{Dim}, and GFP^{Bright} populations at 5 dpf (left) and 12 dpf (right). Data were examined by one-way ANOVA with Sidak's multiple comparisons test. 300 cells quantified for each group over 3 independent experiments. Scale 20 μm. Mean ± SEM represented throughout. $^{****}p < 0.0001$; $^{**}p < 0.01$; $^{*}p < 0.05$.

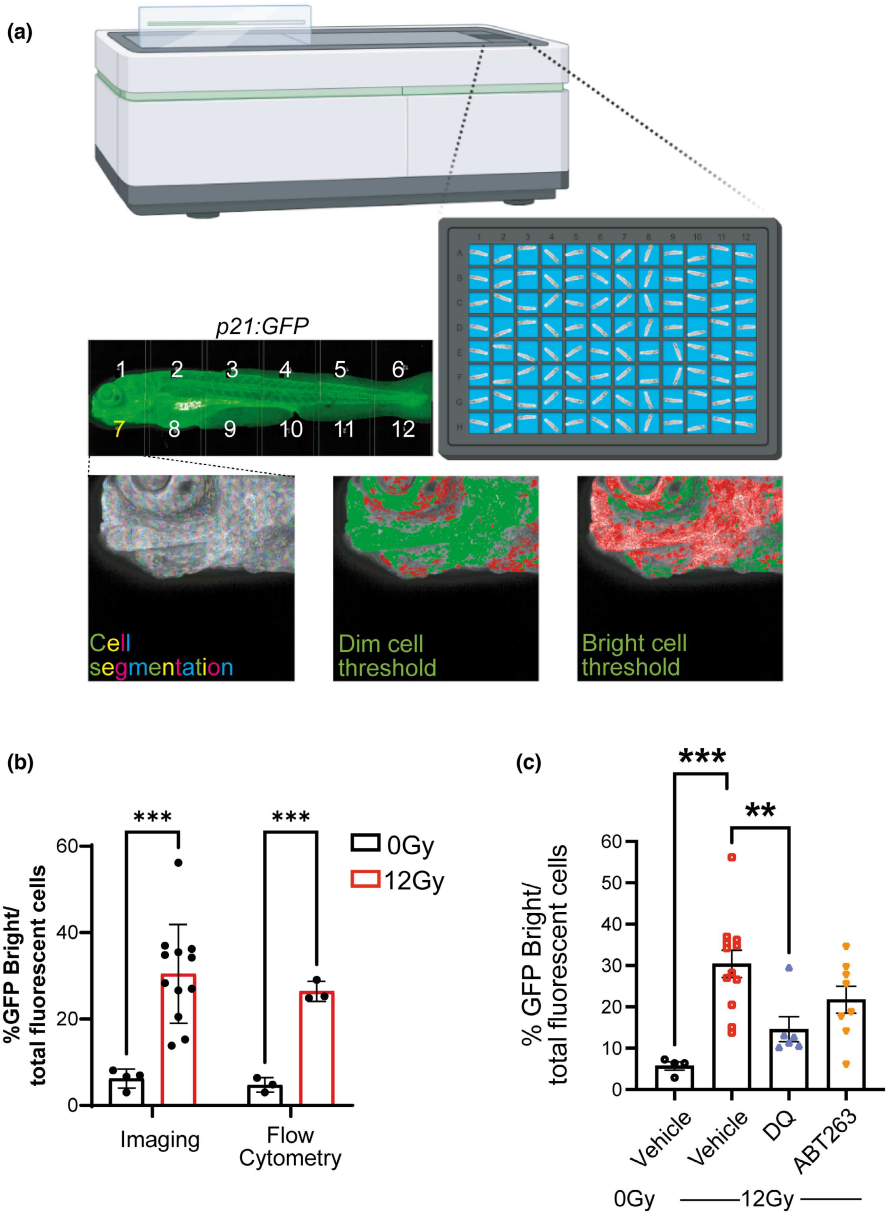

FIGURE 5 Senolytics reduces the number of p21:GFP^{Bright} cells. (a) Diagram representing automated imaging method for p21:GFP zebrafish using The Opera Phenix High-Content Screening System. Tiled confocal photomicrographs from Opera Phenix microscope of 5 dpf p21:GFP zebrafish were acquired, and individual cells were segregated for analysis. The mean fluorescence intensity of individual cells was classified against a threshold set on the basis of level of fluorescence in wild-type fish and non-irradiated p21:GFP fish to identify the GFP^{Bright} population; (b) Percentage of GFP^{Bright} cells calculated by Opera Phenix High-Content Imaging and Flow Cytometry analysis, as a proportion of total fluorescent cells in p21:GFP fish with or without irradiation. (c) Quantification of the proportion of GFP^{Bright} at 5 dpf in laterally oriented p21:GFP fish following irradiation at 2 dpf and treatment starting at 3 dpf with vehicle, dasatinib (D) plus quercetin (Q) or ABT263 (navitoclax). Data were examined with one-way ANOVA with Tukey's multiple comparison's test. Data (from two independent experiments are presented as Mean ± SEM presented. $^{***}p < 0.001$; $^{**}p < 0.01$.

zebrafish are similar to the level of senescence reported in the literature in other species. For example we have found about 0.8% of p21:GFP^{bright} cells in geriatric fish brain and a study in human brains with various levels of Alzheimer's disease found <2% of cells were senescent (Dehkordi et al., 2021). We have identified approximately 4% of GFP^{+} cells in zebrafish liver at 18 months of age. This was similar to the findings of Ogrodnik et al., 2017 in the liver of mice at a similar age (Ogrodnik et al., 2017). The function of the p21^{dim} population is less clear. p21 is a cell cycle regulator, and therefore, the most likely explanation is that it is expressed by a variety of non-senescent cells at very low level. An alternative more speculative explanation is that these cells are on the way to become senescent or are senescent cells, involved in delivering the beneficial effects of senescence during regeneration such as

those described in wound healing. Zebrafish is a highly regenerative organism so it would not be surprising if this were the case. Future work will compare the gene expression profile and function of these two population.

We have established a rapid protocol for the induction of senescence in zebrafish larvae using irradiation. This is a well-known method for rapid induction of senescence in cells, and it has been shown to accelerate signs of ageing such as frailty in mice (Fielder et al., 2019). Previous work in zebrafish showed that irradiation at 1 dpf led to high levels of mortality and developmental abnormalities, similar to our findings (Honjo & Ichinohe, 2019; Zhao et al., 2019). However, we have identified a treatment window using 12 Gy at day 2, which does not cause significant acute toxicity and death. Expression of senescent marker p21 and SA-β-gal could be detected by 5 dpf in approximately similar areas although not perfectly overlapping. This is not surprising as it is known that SA-β-Gal is not increased uniquely in senescent cells (Yang & Hu, 2005) and there is evidence that markers of senescence do not perfectly overlap in all cell types as it has been shown in the case of expression of p16 and p21 (Chandra et al., 2022). The staining was particularly strong in the pharyngeal arches, brain and intestinal regions. This was similar to findings of Da Silva-Álvarez et al. (2020), Kishi et al. (2008) during the identification of mutants expressing higher levels of SA-β-Gal. The mutant genes were involved in regulation of lifespan and telomere length regulation, and showed accelerated signs of ageing in adult life, suggesting the presence of bona fide senescence (Kishi et al., 2008). Whilst this protocol is convenient, it is important to remember that senescence can be obtained as a result of different inducers (replication exhaustion, stress induced and oncogene induced) and it is still unclear how cells obtained in this way compare to those present in naturally-aged organisms. Transcriptomic analysis shows the expression of a group of core genes common to all inducers. However, there are also inducer-specific genes, (Casella et al., 2019), suggesting the need to test any new compound with different models. Models of replicative induced senescence such as *tert*$^{-/-}$ zebrafish line are available for this (Henriques et al., 2013). Similarly, oncogene-induced senescence can be studied by injecting Ras^{G12V} cells in the larval zebrafish epithelia (Haraoka et al., 2022), increasing the potential use of this model. These models give the opportunity to compare the similarities in transcription profile of senescent cells induced by irradiation or other factors in larvae and those found in aged organisms.

We have chosen to develop the model in zebrafish at the larval stage due to the many advantages that this model offers to test gene function or screening new compounds, and which are complementary to those of mammalian systems. As well as high fecundity and ready genetic manipulation, most organs are developed by 48–72 h. By 96 h, the pancreas, liver and gallbladder are developed, and by 120 h, the development of the gastrointestinal system is complete (Cassar et al., 2020; van Wijk et al., 2016). Most organs perform a similar function to the human counterpart with well-conserved physiological mechanisms (Cassar et al., 2020). This means that it is possible to obtain important information on organ function, mechanisms of action and on efficacy and toxicity of compounds. When compared to in vitro cell testing, the model has the added value of taking into consideration the complexities of interactions at the whole organism level. A number of tests are available to assess organ function. We have shown that larvae lose locomotor function with irradiation and there are changes in muscle fibres, which resemble those found in geriatric fish. Locomotion is not just the result of muscle function but requires an integrated response involving brain function, the nervous system and visual acuity. There are other tests available to monitor the fitness of the major organ systems, including heart, memory and cognition, liver, kidney, immune and sensorial function (Cassar et al., 2020).

Their small dimensions mean that each fish can easily fit in a 96-well plate, making any test relatively easy and inexpensive, requiring only small amounts of drugs. For these reasons, use of zebrafish for in vivo drug testing and toxicology is increasing. Whilst it is acknowledged that there are problems of poor solubility with some compounds and it is difficult to compare how toxic in-water dosing relates to mammalian plasma levels, ways to measure absorption, distribution, metabolism and excretion (ADME) in zebrafish are in development (Grech et al., 2019). There is good agreement with findings in mammalian developmental toxicity studies reaching up to 85 (Gustafson et al., 2012) or 87% (Brannen et al., 2010) agreement. Eight molecules are undergoing clinical testing following a combination of human genetic data and testing in zebrafish models without additional animal testing (Patton et al., 2021). There has been an acceleration in technical development to use this model for drug testing in the last 15 years, with development of many animal models of diseases, transgenic lines, tests for cardiac, nephron and liver toxicity (Patton et al., 2021), which makes it a real promise for the future.

The transparency at the larval stage and the availability of reporter lines means that it is possible to isolate cells by flow cytometry or image them at the single-cell level in the living organism, opening up opportunities for mechanistic studies in senescence. There are over 8000 transgenic lines with fluorescent reporters, which model specific diseases, label molecules, specific organelles or specific cell types, allowing their visualisation and tracking in vivo (Choe et al., 2021). For example, there are transgenic lines labelling most cell types of the immune system (Martins et al., 2019). This opens opportunities to visualise and track in real time over a 24 h period the interaction of SC with immune cells in steady state or during regeneration. It will allow us to answer fundamental questions as to whether immune cells are responsible for the elimination of SC, whether this ability is reduced with age and what is their relative contribution to the accumulation of SC with age. We have demonstrated that, using this model, it is possible to identify p21:GFP^{bright} cells using imaging of individual fish in 96-well plates and at the single-cell level, which reflect values observed by flow cytometry with good reproducibility. Both treatments, DQ and navitoclax induced a reduction in p21:GFP^{bright} cells at doses in the same range of what was previously published in cells in vitro, although navitoclax was less effective and did not reach statistical significance. This is similar to previously published findings in cells in

other species. Quercetin showed senolytic properties at 10–20 μM in human adipocytes and endothelial cells and at 100 μM in mouse mesenchymal stem cells (Zhu et al., 2015). Dasatinib was given at concentrations ranging from 100–300 nM in human adipocytes and endothelial cells and 500 nM in mouse mesenchymal stem cells (Zhu et al., 2015). For Navitoclax, there was a narrower range of concentration available before induction of toxicity. The biggest difference between non-senescent and SC was observed at higher concentrations than the one we could use in zebrafish larvae (5 μM vs 10–20 μM; Cai et al., 2020). In addition, Cai et al. (2020) compared the senolytic activity of DQ and navitoclax and senolytic effects were observed in human embryonic fibroblasts and human umbilical vein cells but not in pre-adipocytes with navitoclax (Cai et al., 2020). This was in contrast to DQ, which was effective in all cell types although with different intensity. The reduced toxicity of DQ combined with a larger spectrum of cells affected may explain the increased effectiveness of DQ in our model. Indeed, navitoclax is best when given at lower doses for a longer time to reduce its toxic effects. Its toxicity is well recognised and new compounds targeting selectively SC are in development to overcome this problem (González-Gualda et al., 2020).

In summary, we demonstrate that the p21:GFP model in zebrafish larvae offers a powerful new tool that could be used to accelerate the study of mechanisms of senescence, its relationship with disease and for drug testing purposes, allowing the selection of only the most promising mechanisms and compounds for study in mammalian models.

4 | MATERIALS AND METHODS

4.1 | Husbandry and irradiation

Zebrafish were housed in accordance with the UK Home Office Licence animal care protocols in the Bateson Centre at The University of Sheffield, UK under standard conditions (Nüsslein-Volhard & Dahm, 2002). Procedures in zebrafish older than 5 dpf were approved by the Home Office (Project License 70/8178). Animals were sacrificed by a schedule 1 method. For other procedures, requiring anaesthesia 168 mg/L of MS222 (Sigma, MO, USA) was used. For irradiation, zebrafish were removed from their chorions at 2 dpf, placed in E3 media (5 mM NaCl, 0.17 mM KCl, 0.33 mM CaCl2, 0.33 mM MgSO4, 0.00001% Methylene Blue) and exposed to Cesium-137. After irradiation, zebrafish received fresh E3 media and returned to a 28°C incubator.

4.2 | Generation of p21: GFP Transgenic line

To generate the p21:GFP reporter transgenic line, we used the DKEY 192-O24 bacterial artificial chromosome (BAC), as per standard protocols (Suster et al., 2011). This is a pIndigo BAC-536 vector encompassing the *p21* locus and containing 100 kbp downstream and 590 kbp upstream sequence from the start codon (ZFIN, 2019). A plasmid containing GFP and a kanamycin resistance cassette, (generated by Dr. Stone Elworthy, The University of Sheffield), amplified with Ultramer DNA oligos (IDT, IA, USA; sequences in Table 1) was used to insert GFP directly after the *p21* locus. A tol2-transposon-mediated system was incorporated according to standard protocols (Suster et al., 2011) t through bacteriophage-mediated homologous recombination using an itol2kan plasmid (generated by Renshaw lab, The University of Sheffield; Table 1). Finally, the modified plasmid was purified using a Nucleobond PC100 kit (Machery-Nagel, Deutschland) as per manufacturers' instructions and quantified. Injections of the modified BAC into single-cell stage *nacre* zebrafish embryos (<30 min post-fertilisation) were carried out. Injected larvae (F0s) were screened for transient GFP expression and raised to identify a stable F1 transgenic line.

TABLE 1 Primer sequences used to modify DKEY-192O24 BAC.

Name	Sequence
GFP targeting construct	Forward – 5′ ATATTTAATGTGATTTTTAC TGTGGTTTGTGTTTGXAGAATTACCGC CATGGTGAGCAAGGGCGAGCTGTTC 3′
	Reverse – 5′ GCCTAGTCGGCCCATTACCG AGTGAACGTAGGATCCGCTTGTGCGCC GCGATATCTGCAGAATTCGCCCTTGA 3′
Tol2 targeting construct	Forward – 5′ AAGCTTAAGTGATCTCCAAA AAATAA 3′
	Reverse – 5′ GAATTCAATACTCAAGTACA ATTTTA 3′

4.3 | Assessment of senescence in whole fish

In situ hybridisation was performed according to standard protocol (Thisse & Thisse, 2008). For *p21* in situ hybridisation, the antisense RNA probe for *p21* was synthesised from linearised plasmid DNA provided by David Whitmore (University College London; Laranjeiro et al., 2013). Imaging was performed by placing larvae in 80%–100% glycerol solution on a glass cover slip (Scientific Laboratory Supplies, UK). Transmitted light imaging was performed using a Nikon SMZ1500 stereomicroscope with a Prior Z-drive and a Nikon DS-Fi1 colour camera with NIS elements software (Version 4.3). For quantitation, colorimetric analysis was chosen by selection of the zebrafish head, excluding the eye and extending as far as the optic vesicle. Blind ranking was carried out. Irradiated and non-irradiated fish were imaged individually and assigned a code using a random integer generator. The images were then ordered according to their staining intensity by an operator based on their visual appearance with the highest ranking assigned to the strongest staining. The codes were then revealed to assign the ranked animals to their group and perform statistical analysis of the ranks by a Kruskal–Wallis. Each dot represents a fish with their ranking.

To assess SA-β-Gal activity in zebrafish larvae, the procedure was carried out as previously described (Kishi et al., 2008). Imaging

and quantification were performed as described for p21 in situ hybridization analysis.

For γH2AX staining in the whole zebrafish, after fixation, fish were then transferred to glass reaction vials and incubated with acetone for 7 min at −20°C Zebrafish were then incubated with histone H2A.XS139ph (phospho Ser139) antibody (Genetex, CA, USA, 1:1000 dilution in blocking solution), followed by Alexa Fluor 568 goat anti-rabbit (Invitrogen, UK, 1:500 dilution in blocking solution) for 2 h at room temperature and mounted with Vectashield (Vector laboratories, UK). The UltraVIEWVoX spinning disc confocal laser imaging system (Perkin Elmer) was used to image the fish, using 1 μM z-stacks with the Prior 200 μm z-piezo. Images were analysed on Volocity™ software (version 6.3). The number of nuclear bright red+ cells was enumerated in 4 regions of interest. At least 300 cells were quantified for each test.

4.4 | qPCR

Zebrafish embryos were homogenised by addition of Trizol (Sigma, USA) and passed through a QIAshredder column (Qiagen, Netherlands). The RNA was then purified; First-Strand cDNA Synthesis was performed using SuperScriptTM II Reverse Transcription kit (Invitrogen, UK) as per manufacturer's instructions. qPCR was performed using MESA GREEN qPCR MasterMix Plus for SYBR® (Eurogentec, UK) and an ABI 7900HT Sequence Detection System (Applied Biosystems, CA, USA). Quantification was carried out by fold expression change following irradiation ($2^{-\Delta\Delta Ct}$, relative to βactin and unirradiated control). Primer sequences are listed in Table 2.

4.5 | Histology of muscle

Adult zebrafish were fixed in 10% buffered formalin for 72 h at 4°C before decalcification in 0.5 M EDTA for 72 h at 4°C. Zebrafish larvae were fixed in 10% buffered formalin for 24 h without decalcification. Fixed zebrafish were then paraffin-embedded, sectioned longitudinally at 3 μm thickness and stained with haematoxylin–eosin (H&E) for histopathological analysis. To analyse the H&E-stained zebrafish, slides were digitised by a Pannoramic 250 Flash II slide scanner (3D Histech, Hungary) at 20× magnification. Zebrafish muscle width was then quantified across the larval tail, or ventral muscle for adult zebrafish.

4.6 | Analysis of locomotion

Locomotor activity was recorded using the Zebrabox (ViewPoint Life Sciences, Lyon, France) tracking system and Zebralab software (ViewPoint Life Sciences, Lyon, France). Zebrafish were placed in a 24-well plate in E3 medium, and movement was recorded for 30 min. Light and dark cycles of 5 min at 100% light and 5 min at 0% light were used to stimulate movement of the fish. Total movement across the 30-min period was assessed with Zebralab.

TABLE 2 Table of primer sequences for qPCR.

Gene	Sequence
βactin	Forward – 5′ TTCACCACCACAGCCGAAAGA 3′
	Reverse – 5′ TACCGCAAGATTCCATACCCA 3′
P21 (cdkn1a)	Forward – 5′ AGGAAAAGCAGCAGAAACG 3′
	Reverse – 5′ TGTTGGTCTGTTTGCGCTT 3′
P16-like (cdkn2a/b)	Forward – 5′ ATGATGAACGTCGAGGATGAACTG 3′
	Reverse – 5′ ATTGGCATTCACTCCGTTAG AAAGT 3′
Il8a	Forward – 5′ GAAAGCCGACGCATTGGAAA 3′
	Reverse – 5′ TTAACCCATGGAGCAGAGGG 3′
Mmp2	Forward – 5′ AGCTTTGACGATGACCG CAAATGG 3′
	Reverse – 5′ GCCAATGGCTTGTCTGTTGGTTCT 3′
Cyclin-g1	Reverse – 5′ CACTGGCCAGAGGGACATTTTTCT 3′
P53	Forward – 5′ GCTTGTCACAGGGGTCATTT 3′
	Reverse – 5′ ACAAAGGTCCCAGTGGAGTG 3′

4.7 | Fluorescent activated cell sorting

Zebrafish larvae were digested with Liberase TL (Roche, UK) at 40 μg/mL, 37°C for 35 min and blocked with 10% foetal bovine serum (FBS) (Sigma-Aldrich, UK). The suspension was then centrifuged at 500 *g* for 5 min, before cells were resuspended in Leibovitz's L15 media (ThermoFisher Scientific Inc., USA), containing 20% FBS and 5 mM EDTA. Cells were incubated with 7-Aminoactinomycin D (7AAD, ThermoFisher Scientific Inc., USA) for 5 min before being examined by a LSRII (BD) flow cytometer (BD Biosciences, San Jose, CA, USA). For the assessment of adult zebrafish organs, they were dissected and manually dissociated with a sterile scalpel before being digested as described above for the zebrafish larvae.

4.8 | Immunofluorescent staining of single cells

Following fluorescent activated cell sorting, p21:GFP cells were fixed with 4% paraformaldehyde for 20 min on ice. Cells were then cytospun at 500*g* for 5 min with medium acceleration onto SuperFrost Ultra Plus™ adhesion slides (ThermoFisher Scientific Inc., USA) and dried overnight at room temperature (22°C). Cells were then permeabilised with 0.5% Triton X-100 (Sigma-Aldrich) for 10 min at room temperature and blocked for 1–2 h at room temperature with 3% Bovine Serum Albumin, 5% Goat Serum, 0.3% Tween-20 in PBS. Slides were then incubated with primary

antibodies overnight at 4°C. A Combination of antibodies against Proliferating Cell Nuclear Antigen (PCNA, Santa Cruz, CA, USA, 1:200 dilution) and histone H2A.XS139ph (phospho Ser139) antibody (Genetex, CA, USA, 1:300 dilution) or Proliferating Cell Nuclear Antigen (PCNA, Santa Cruz, CA, USA, 1:200 dilution) and IL6 (Abcam, MA, USA, 1:500 dilution) were used. This was followed by overnight incubation with secondary antibodies at 4°C in blocking solution. Combinations of antibodies against Alexa Fluor 488 goat anti-chicken (Abcam, MA, USA, 1 in 500 dilution), Alexa Fluor 568 goat anti-rabbit (Invitrogen, UK, 1:500 dilution) and Alexa Fluor 647 goat anti-mouse (Invitrogen, UK, 1:500 dilution) were used. Slides were stained with DAPI (Sigma-Aldrich, UK, 1:2000 dilution in PBS) and then mounted in Vectashield (Vector laboratories, UK). Slides were imaged on a Deltavision microscope using an UplanSApo 40x oil objective (NA 1.3) and Photometrics CoolsnapHQ CCD camera. Z stacks were imaged at 1 µm, and deconvolution software was used for the pγH2AX staining to make the foci more visible. Excitation by a 100 W Hg lamp was used. Quantification was carried out with maximum intensity projections of 15 z-stacks (15 µm thickness). Cells with 5 or more γH2AX foci in a single nucleus were deemed positive (stained with DAPI). Cells positive for IL6 had clear red fluorescence in the regions around the nucleus, whilst cells positive for PCNA had clear nuclear staining. At least 300 cells were quantified per group.

4.9 | Opera Phenix imaging

Zebrafish were dechorionated and irradiated at 2 dpf. At 3 dpf, zebrafish were placed in individual wells of a 96-well µclear® cell culture imaging plates, containing either the senolytic cocktail Dasatinib (D, 500 nM) and Quercetin (Q, 50 µM) or ABT-263 (Navitoclax, 5 µM), dissolved in 0.5% DMSO which was used as vehicle control. At 4 dpf, the drug media was refreshed. At 5 dpf, zebrafish were anaesthetised and imaged on an Opera Phenix® High-Content Screening System (Perkin Elmer). The 96 wells were first imaged at 5× magnification to identify zebrafish via their GFP intensity, before a 20× high magnification z-stack was taken of the whole zebrafish larvae. Images of 5 dpf zebrafish were quantified on Harmony® High-Content Imaging and Analysis Software. To first identify our region of interest, the whole zebrafish, the 'Common Threshold' method was used on the Alexa 488 channel to detect GFP intensity. A threshold of 0.25 was used to determine the mean fluorescence intensity of p21:GFP zebrafish. To identify and segregate cells, method 'M' was utilised with a diameter of 20 µM, splitting sensitivity at 0.48, and common threshold at 0.22. The intensity properties of individual cells are analysed to threshold GFP^{Dim} and GFP^{Bright} cells. GFP^{Bright} cells have a mean Alex 488 intensity of at least 1250, whilst dim cells have an intensity between 400 and 1250. This was established using untreated wild-type zebrafish, 0 Gy and 12 Gy irradiated zebrafish, before results were compared to flow cytometry data Next, the number of GFP^{Dim} and GFP^{Bright} cells in the 5 dpf zebrafish was automatically counted.

4.10 | Statistical analysis

Data were analysed by Prism software (version 8.1). Data were analysed by *t*-test or one-way ANOVA. Analysis and post hoc tests carried out for individual data sets are specified in their respective figure legends with significance $^{*}p<0.05$, $^{**}p<0.01$, $^{***}p<0.001$, $^{****}p<0.0001$.

AUTHOR CONTRIBUTION

SM designed and performed the experiments, analysed the data, wrote and approved the manuscript; PMS and CMH designed the experiments on detection of DNA damage, reviewed and approved the manuscript; HM designed the experiment for testing the senolytics, reviewed and approved the manuscript; SB designed the experiment to test muscle function, reviewed and approved the manuscript; CL and SAR designed the experiment for the generation of the p21 transgenic zebrafish, reviewed and approved the manuscript. IB conceived the idea, designed the experiments, wrote and approved the manuscript.

ACKNOWLEDGMENTS

Samir Morsli was funded by the Biotechnology and Biological Sciences Research councils PhD studentship (DTP2 BBSRC Grant Ref: BB/M011151/1). This research (Heather Mortiboys) was supported/funded by the NIHR Sheffield Biomedical Research Centre (BRC)/NIHR Sheffield Clinical Research Facility (CRF). Stephen Renshaw's contribution was supported by the Medical Research Council/Versus Arthritis Centre for Integrated Research into Musculoskeletal Ageing (R/P020941/1). The views expressed are those of the author(s) and not necessarily those of the NHS, the NIHR or the Department of Health and Social Care (DHSC). Figure 5, Figure S3 and graphical abstract were created with BioRender.com. We are grateful to Stone Elworthy for providing the GFP plasmid and David Whitmore (University College London) for providing the p21 probe.

CONFLICT OF INTEREST STATEMENT

No conflict of interest to declare.

DATA AVAILABILITY STATEMENT

All data and the p21GFP transgenic line will be available upon request.

ORCID

Samir Morsli https://orcid.org/0000-0002-0371-0732
Catarina M. Henriques https://orcid.org/0000-0003-1882-756X
Ilaria Bellantuono https://orcid.org/0000-0001-9994-6987

REFERENCES

Biran, A., Zada, L., Abou Karam, P., Vadai, E., Roitman, L., Ovadya, Y., Porat, Z., & Krizhanovsky, V. (2017). Quantitative identification of senescent cells in aging and disease. *Aging Cell*, *16*(4), 661–671. https://doi.org/10.1111/acel.12592

Bradford, Y. M., Toro, S., Ramachandran, S., Ruzicka, L., Howe, D. G., Eagle, A., Kalita, P., Martin, R., Taylor Moxon, S. A., Schaper, K., & Westerfield, M. (2017). Zebrafish models of human disease: Gaining insight into human disease at ZFIN. *ILAR Journal*, *58*(1), 4–16. https://doi.org/10.1093/ilar/ilw040

Brannen, K. C., Panzica-Kelly, J. M., Danberry, T. L., & Augustine-Rauch, K. A. (2010). Development of a zebrafish embryo teratogenicity assay and quantitative prediction model. *Birth Defects Research. Part B, Developmental and Reproductive Toxicology*, *89*(1), 66–77. https://doi.org/10.1002/bdrb.20223

Cai, Y., Zhou, H., Zhu, Y., Sun, Q., Ji, Y., Xue, A., Wang, Y., Chen, W., Yu, X., Wang, L., Chen, H., Li, C., Luo, T., & Deng, H. (2020). Elimination of senescent cells by β-galactosidase-targeted prodrug attenuates inflammation and restores physical function in aged mice. *Cell Research*, *30*(7), 574–589. https://doi.org/10.1038/s41422-020-0314-9

Carneiro, M. C., Henriques, C. M., Nabais, J., Ferreira, T., Carvalho, T., & Ferreira, M. G. (2016). Short telomeres in key tissues initiate local and systemic aging in zebrafish. *PLoS Genetics*, *12*(1), e1005798. https://doi.org/10.1371/journal.pgen.1005798

Casella, G., Munk, R., Kim, K. M., Piao, Y., De, S., Abdelmohsen, K., & Gorospe, M. (2019). Transcriptome signature of cellular senescence. *Nucleic Acids Research*, *47*(14), 7294–7305. https://doi.org/10.1093/nar/gkz555

Cassar, S., Adatto, I., Freeman, J. L., Gamse, J. T., Iturria, I., Lawrence, C., Muriana, A., Peterson, R. T., van Cruchten, S., & Zon, L. I. (2020). Use of zebrafish in drug discovery toxicology. *Chemical Research in Toxicology*, *33*(1), 95–118. https://doi.org/10.1021/acs.chemrestox.9b00335

Cesari, M., Leeuwenburgh, C., Lauretani, F., onder, G., Bandinelli, S., Maraldi, C., Guralnik, J. M., Pahor, M., & Ferrucci, L. (2006). Frailty syndrome and skeletal muscle: Results from the Invecchiare in chianti study. *The American Journal of Clinical Nutrition*, *83*(5), 1142–1148. https://doi.org/10.1093/ajcn/83.5.1142

Chandra, A., Lagnado, A. B., Farr, J. N., Doolittle, M., Tchkonia, T., Kirkland, J. L., LeBrasseur, N. K., Robbins, P. D., Niedernhofer, L. J., Ikeno, Y., Passos, J. F., Monroe, D. G., Pignolo, R. J., & Khosla, S. (2022). Targeted clearance of p21- but not p16-positive senescent cells prevents radiation-induced osteoporosis and increased marrow adiposity. *Aging Cell*, *21*(5), e13602. https://doi.org/10.1111/acel.13602

Choe, C. P., Choi, S.-Y., Kee, Y., Kim, M. J., Kim, S.-H., Lee, Y., Park, H. C., & Ro, H. (2021). Transgenic fluorescent zebrafish lines that have revolutionized biomedical research. *Laboratory Animal Research*, *37*(1), 26. https://doi.org/10.1186/s42826-021-00103-2

Da Silva-Álvarez, S., Guerra-Varela, J., Sobrido-Cameán, D., Quelle, A., Barreiro-Iglesias, A., Sánchez, L., & Collado, M. (2020). Developmentally-programmed cellular senescence is conserved and widespread in zebrafish. *Aging*, *12*(18), 17895–17901. https://doi.org/10.18632/aging.103968

Dehkordi, S. K., Walker, J., Sah, E., Bennett, E., Atrian, F., Frost, B., Woost, B., Bennett, R. E., Orr, T. C., Zhou, Y., Andhey, P. S., Colonna, M., Sudmant, P. H., Xu, P., Wang, M., Zhang, B., Zare, H., & Orr, M. E. (2021). Profiling senescent cells in human brains reveals neurons with CDKN2D/p19 and tau neuropathology. *Nature Aging*, *1*(12), 1107–1116. https://doi.org/10.1038/s43587-021-00142-3

Di Micco, R., Krizhanovsky, V., Baker, D., & d'Adda di Fagagna, F. (2021). Cellular senescence in ageing: From mechanisms to therapeutic opportunities. *Nature Reviews Molecular Cell Biology*, *22*(2), 75–95. https://doi.org/10.1038/s41580-020-00314-w

Ellett, F., Pase, L., Hayman, J. W., Andrianopoulos, A., & Lieschke, G. J. (2011). mpeg1 promoter transgenes direct macrophage-lineage expression in zebrafish. *Blood*, *117*(4), e49–e56. https://doi.org/10.1182/blood-2010-10-314120

Fielder, E., Weigand, M., Agneessens, J., Griffin, B., Parker, C., Miwa, S., & von Zglinicki, T. (2019). Sublethal whole-body irradiation causes progressive premature frailty in mice. *Mechanisms of Ageing and Development*, *180*, 63–69. https://doi.org/10.1016/j.mad.2019.03.006

González-Gualda, E., Baker, A. G., Fruk, L., & Muñoz-Espín, D. (2021). A guide to assessing cellular senescence in vitro and in vivo. *The FEBS Journal*, *288*(1), 56–80. https://doi.org/10.1111/febs.15570

González-Gualda, E., Pàez-Ribes, M., Lozano-Torres, B., Macias, D., Wilson, J. R., 3rd, González-López, C., Ou, H. L., Mirón-Barroso, S., Zhang, Z., Lérida-Viso, A., Blandez, J. F., Bernardos, A., Sancenón, F., Rovira, M., Fruk, L., Martins, C. P., Serrano, M., Doherty, G. J., Martínez-Máñez, R., & Muñoz-Espín, D. (2020). Galacto-conjugation of Navitoclax as an efficient strategy to increase senolytic specificity and reduce platelet toxicity. *Aging Cell*, *19*(4), e13142. https://doi.org/10.1111/acel.13142

Grech, A., Tebby, C., Brochot, C., Bois, F. Y., Bado-Nilles, A., Dorne, J. L., Quignot, N., & Beaudouin, R. (2019). Generic physiologically-based toxicokinetic modelling for fish: Integration of environmental factors and species variability. *Science of the Total Environment*, *651*(Pt 1), 516–531. https://doi.org/10.1016/j.scitotenv.2018.09.163

Gustafson, A. L., Stedman, D. B., Ball, J., Hillegass, J. M., Flood, A., Zhang, C. X., Panzica-Kelly, J., Cao, J., Coburn, A., Enright, B. P., Tornesi, M. B., Hetheridge, M., & Augustine-Rauch, K. A. (2012). Inter-laboratory assessment of a harmonized zebrafish developmental toxicology assay – progress report on phase I. *Reproductive Toxicology*, *33*(2), 155–164. https://doi.org/10.1016/j.reprotox.2011.12.004

Haraoka, Y., Akieda, Y., Nagai, Y., Mogi, C., & Ishitani, T. (2022). Zebrafish imaging reveals TP53 mutation switching oncogene-induced senescence from suppressor to driver in primary tumorigenesis. *Nature Communications*, *13*(1), 1417. https://doi.org/10.1038/s41467-022-29061-6

Henriques, C. M., Carneiro, M. C., Tenente, I. M., Jacinto, A., & Ferreira, M. G. (2013). Telomerase is required for zebrafish lifespan. *PLoS Genetics*, *9*(1), e1003214. https://doi.org/10.1371/journal.pgen.1003214

Honjo, Y., & Ichinohe, T. (2019). Cellular responses to ionizing radiation change quickly over time during early development in zebrafish. *Cell Biology International*, *43*(5), 516–527. https://doi.org/10.1002/cbin.11117

Howe, K., Clark, M. D., Torroja, C. F., Torrance, J., Berthelot, C., Muffato, M., Collins, J. E., Humphray, S., McLaren, K., Matthews, L., McLaren, S., Sealy, I., Caccamo, M., Churcher, C., Scott, C., Barrett, J. C., Koch, R., Rauch, G. J., White, S., … Stemple, D. L. (2013). The zebrafish reference genome sequence and its relationship to the human genome. *Nature*, *496*(7446), 498–503. https://doi.org/10.1038/nature12111

Jurk, D., Wilson, C., Passos, J. F., Oakley, F., Correia-Melo, C., Greaves, L., Saretzki, G., Fox, C., Lawless, C., Anderson, R., Hewitt, G., Pender, S. L. F., Fullard, N., Nelson, G., Mann, J., van de Sluis, B., Mann, D. A., & von Zglinicki, T. (2014). Chronic inflammation induces telomere dysfunction and accelerates ageing in mice. *Nature Communications*, *5*(1), 4172. https://doi.org/10.1038/ncomms5172

Kishi, S., Bayliss, P. E., Uchiyama, J., Koshimizu, E., Qi, J., Nanjappa, P., Imamura, S., Islam, A., Neuberg, D., Amsterdam, A., & Roberts, T. M. (2008). The identification of zebrafish mutants showing alterations in senescence-associated biomarkers. *PLoS Genetics*, *4*(8), e1000152. https://doi.org/10.1371/journal.pgen.1000152

Laranjeiro, R., Tamai, T. K., Peyric, E., Krusche, P., Ott, S., & Whitmore, D. (2013). Cyclin-dependent kinase inhibitor p20 controls circadian cell-cycle timing. *Proceedings of the National Academy of Sciences of the United States of America*, *110*(17), 6835–6840. https://doi.org/10.1073/pnas.1217912110

Martins, R. R., Ellis, P. S., MacDonald, R. B., Richardson, R. J., & Henriques, C. M. (2019). Resident immunity in tissue repair and maintenance: The zebrafish model coming of age. *Frontiers in Cell and Developmental Biology*, *7*, 12. https://doi.org/10.3389/fcell.2019.00012

Nüsslein-Volhard, C., & Dahm, R. (2002). *Zebrafish: A practical approach* (p. 303). Oxfrod University press.

Ogrodnik, M., Miwa, S., Tchkonia, T., Tiniakos, D., Wilson, C. L., Lahat, A., Day, C. P., Burt, A., Palmer, A., Anstee, Q. M., Grellscheid, S. N., Hoeijmakers, J. H. J., Barnhoorn, S., Mann, D. A., Bird, T. G., Vermeij, W. P., Kirkland, J. L., Passos, J. F., von Zglinicki, T., & Jurk, D. (2017). Cellular senescence drives age-dependent hepatic steatosis. *Nature Communications*, *8*(1), 15691. https://doi.org/10.1038/ncomms15691

Patton, E. E., Zon, L. I., & Langenau, D. M. (2021). Zebrafish disease models in drug discovery: From preclinical modelling to clinical trials. *Nature Reviews Drug Discovery*, *20*(8), 611–628. https://doi.org/10.1038/s41573-021-00210-8

Renshaw, S. A., Loynes, C. A., Trushell, D. M., Elworthy, S., Ingham, P. W., & Whyte, M. K. (2006). A transgenic zebrafish model of neutrophilic inflammation. *Blood*, *108*(13), 3976–3978. https://doi.org/10.1182/blood-2006-05-024075

Robbins, P. D., Jurk, D., Khosla, S., Kirkland, J. L., LeBrasseur, N. K., Miller, J. D., Passos, J. F., Pignolo, R. J., Tchkonia, T., & Niedernhofer, L. J. (2021). Senolytic drugs: Reducing senescent cell viability to extend health span. *Annual Review of Pharmacology and Toxicology*, *61*(1), 779–803. https://doi.org/10.1146/annurev-pharmtox-050120-105018

Shim, J., Choi, J.-H., Park, M.-H., Kim, H., Kim, J. H., Kim, S.-Y., Hong, D., Kim, S., Lee, J. E., Kim, C. H., Lee, J. S., & Bae, Y. K. (2017). Development of zebrafish medulloblastoma-like PNET model by TALEN-mediated somatic gene inactivation. *Oncotarget*, *8*(33), 55280–55297.

Suster, M. L., Abe, G., Schouw, A., & Kawakami, K. (2011). Transposon-mediated BAC transgenesis in zebrafish. *Nature Protocols*, *6*(12), 1998–2021. https://doi.org/10.1038/nprot.2011.416

Thisse, C., & Thisse, B. (2008). High-resolution in situ hybridization to whole-mount zebrafish embryos. *Nature Protocols*, *3*(1), 59–69. https://doi.org/10.1038/nprot.2007.514

van Wijk, R. C., Krekels, E. H. J., Hankemeier, T., Spaink, H. P., & van der Graaf, P. H. (2016). Systems pharmacology of hepatic metabolism in zebrafish larvae. *Drug Discovery Today: Disease Models*, *22*, 27–34. https://doi.org/10.1016/j.ddmod.2017.04.003

von Hellfeld, R., Brotzmann, K., Baumann, L., Strecker, R., & Braunbeck, T. (2020). Adverse effects in the fish embryo acute toxicity (FET) test: A catalogue of unspecific morphological changes versus more specific effects in zebrafish (Danio rerio) embryos. *Environmental Sciences Europe*, *32*(1), 122. https://doi.org/10.1186/s12302-020-00398-3

Wang, B., Wang, L., Gasek, N. S., Zhou, Y., Kim, T., Guo, C., Jellison, E. R., Haynes, L., Yadav, S., Tchkonia, T., Kuchel, G. A., Kirkland, J. L., & Xu, M. (2021). An inducible p21-Cre mouse model to monitor and manipulate p21-highly-expressing senescent cells in vivo. *Nature Aging*, *1*(10), 962–973. https://doi.org/10.1038/s43587-021-00107-6

Wang, G., Rajpurohit, S. K., Delaspre, F., Walker, S. L., White, D. T., Ceasrine, A., Kuruvilla, R., Li, R. J., Shim, J. S., Liu, J. O., Parsons, M. J., & Mumm, J. S. (2015). First quantitative high-throughput screen in zebrafish identifies novel pathways for increasing pancreatic β-cell mass. *eLife*, *4*. https://doi.org/10.7554/eLife.08261

Wang, L., Wang, B., Gasek, N. S., Zhou, Y., Cohn, R. L., Martin, D. E., Zuo, W., Flynn, W. F., Guo, C., Jellison, E. R., Kim, T., Prata, L. G. P. L., Palmer, A. K., Li, M., Inman, C. L., Barber, L. S., al-Naggar, I. M. A., Zhou, Y., du, W., … Xu, M. (2022). Targeting p21(Cip1) highly expressing cells in adipose tissue alleviates insulin resistance in obesity. *Cell Metabolism*, *34*(1), 75–89.e8. https://doi.org/10.1016/j.cmet.2021.11.002

Yang, N. C., & Hu, M. L. (2005). The limitations and validities of senescence associated-beta-galactosidase activity as an aging marker for human foreskin fibroblast Hs68 cells. *Experimental Gerontology*, *40*(10), 813–819. https://doi.org/10.1016/j.exger.2005.07.011

Yousefzadeh, M. J., Zhao, J., Bukata, C., Wade, E. A., McGowan, S. J., Angelini, L. A., Bank, M. P., Gurkar, A. U., McGuckian, C., Calubag, M. F., Kato, J. I., Burd, C. E., Robbins, P. D., & Niedernhofer, L. J. (2020). Tissue specificity of senescent cell accumulation during physiologic and accelerated aging of mice. *Aging Cell*, *19*(3), e13094. https://doi.org/10.1111/acel.13094

ZFIN. (2019). *cdkn1a, Zebrafish Information Network (ZFIN)*. https://zfin.org/ZDB-GENE-070705-7

Zhao, W., Hu, N., Ding, D., Long, D., Li, S., Li, G., & Zhang, H. (2019). Developmental toxicity and apoptosis in zebrafish embryos induced by low-dose γ-ray irradiation. *Environmental Science and Pollution Research International*, *26*(4), 3869–3881. https://doi.org/10.1007/s11356-018-3893-y

Zhu, Y., Tchkonia, T., Pirtskhalava, T., Gower, A. C., Ding, H., Giorgadze, N., Palmer, A. K., Ikeno, Y., Hubbard, G. B., Lenburg, M., O'Hara, S. P., LaRusso, N., Miller, J. D., Roos, C. M., Verzosa, G. C., LeBrasseur, N., Wren, J. D., Farr, J. N., Khosla, S., … Kirkland, J. L. (2015). The Achilles' heel of senescent cells: From transcriptome to senolytic drugs. *Aging Cell*, *14*(4), 644–658. https://doi.org/10.1111/acel.12344

SUPPORTING INFORMATION

Additional supporting information can be found online in the Supporting Information section at the end of this article.

How to cite this article: Morsli, S., Henriques, C. M., Ellis, P. S., Mortiboys, H., Baxendale, S., Loynes, C. A., Renshaw, S. A., & Bellantuono, I. (2023). A p21-GFP zebrafish model of senescence for rapid testing of senolytics in vivo. *Aging Cell*, *00*, e013835. https://doi.org/10.1111/acel.13835